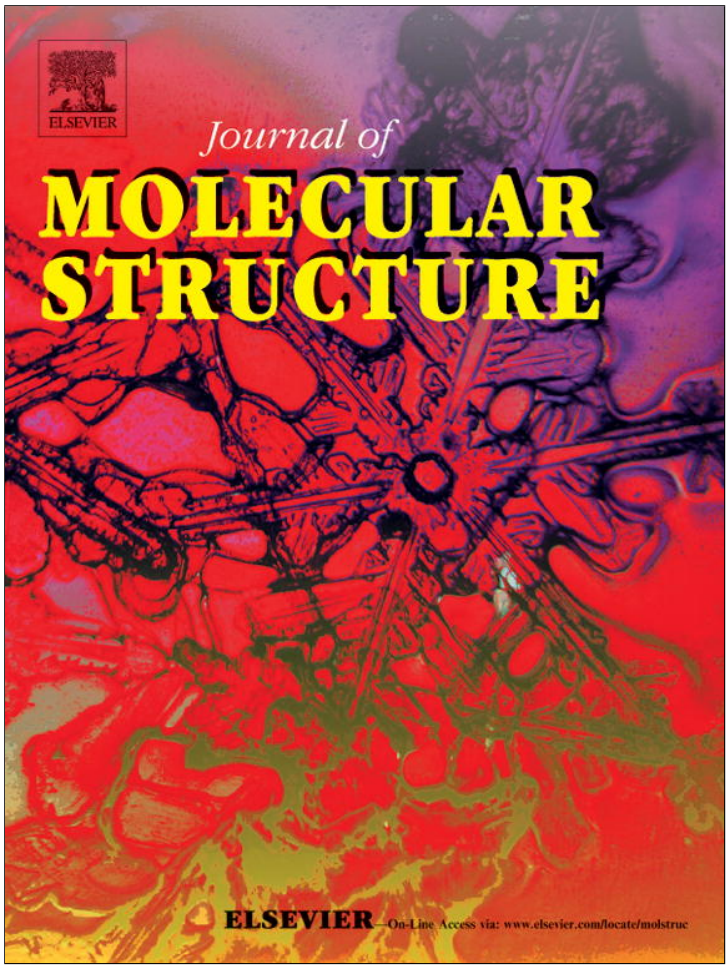

(This is a sample cover image for this issue. The actual cover is not yet available at this time.)

Journal of Molecular Structure 1036 (2013) 133–143

Contents lists available at SciVerse ScienceDirect

Journal of Molecular Structure

journal homepage: www.elsevier.com/locate/molstruc

Stereochemistry of C7-allyl yohimbine explored by X-ray crystallography

Natsuko Kagawa [a,*], Yoshitake Masuda [b], Tsumoru Morimoto [a], Kiyomi Kakiuchi [a]

[a] Graduate School of Materials Science, Nara Institute of Science and Technology (NAIST), Ikoma, Nara 630-0192, Japan
[b] National Institute of Advanced Industrial Science and Technology (AIST), Nagoya 463-8560, Japan

HIGHLIGHTS

- An indole in yohimbine was directly allylated by cat. Pd(0) into a 3*H*-indole.
- X-ray crystallographic analysis revealed the solid structure of (7*R*)-allyl yohimbine.
- Steric effects dominate stereoselective approach of the π-allyl Pd complex.

ARTICLE INFO

Article history:
Received 2 August 2012
Received in revised form 27 September 2012
Accepted 27 September 2012
Available online 11 October 2012

Keywords:
Palladium
Allylation
3*H*-Indole
Indole alkaloids
Yohimbine
Reserpine

ABSTRACT

X-ray crystallographic analysis revealed that the palladium-catalyzed β-allylation of yohimbine proceeded in a (7*S*)-selective manner. The crystal structure had an indolenine unit that was generally unstable in air. A stereoselective outcome was obtained when the palladium π-allyl complex approached yohimbine from the less-hindered *pro-S* side. However, during reserpine allylation—because the structure of reserpine is that of a *transoid*-3, 15-ring junction—the palladium π-allyl complex approached from both sides: *pro-S* and *pro-R*. A computational method was developed to discuss this selectivity. Experimental details and considerations of the reaction are provided.

1. Introduction

Indolenine **1** (3*H*-indole) is a 1,3-tautomer of indole **2** (Scheme 1) [1] with a life that is too short to isolate, because it lacks aromatic stability—according to Hückel's rule. However, indolenine-derived molecules are prevalent structural motifs in natural products [2–3], medicinal compounds [4], and organic materials [5]. In particular, cyanine dyes containing indolenium salts are widely used for labeling DNA due to their fluorescent properties [6]. The structure of indolenine possesses several chemical characteristics that have attracted the interest of scientists: a reducible phenyl imino group (Ph—N=C), an acidic methylene unit on C3, and a basic lone pair of electrons on N1. Anionic indolenine **3** may reach aromatic stability when indole is treated with a metal base, because **3** is a resonance structure of anionic indole **4**. Employing this feature, many researchers have reported regioselective β(C3)-alkylation of indole under strong basic conditions [7]. In the literature, although the value of the electron density at the N1(α) position of the indole anion **4** is larger than that at the C3(β) position of the indolenine anion **3**, the regioselectivity of α- and β-alkylation was changed remarkably by the effect of counter metal ions. A potassium base is used as a reagent for the selective α-alkylation of indole, and a magnesium base is utilized for the selective β-alkylation of indole.

The basic β-alkylation of indole cannot stop promoting the reaction at the point of 3-monosubstituted indolenine **5** as an intermediate, which turns into 3-substituted indole **6** through rapid tautomerization (Scheme 2). For the synthesis of isolable 3,3-disubstituted indolenine **8**, we chose 3-alkylindole **7** as a starting material, a Grignard reagent as a magnesium base, and allyl bromide as an electrophile. The allyl bromide is one of the most reactive electrophilic reagents in such an alkylation, and ^{1}H NMR signals of allyl moieties are easily detected and identified. Indoles **7** were treated with a Grignard reagent and then allyl bromide to give indolenines **8** in a highly β-selective manner. However, obtained indolenines were unstable in air, and worse yet, they stuck to the silica gel upon purification. Therefore, a constant yield of the

* Corresponding author. Present address: Graduate School of Pharmaceutical Sciences, Chiba University, 1-8-1 Inohana, Chuo, Chiba 260-8675, Japan. Tel./fax: +81 43 226 2945.
E-mail address: knatsuko@faculty.chiba-u.jp (N. Kagawa).

0022-2860/$ - see front matter © 2012 Elsevier B.V. All rights reserved.
http://dx.doi.org/10.1016/j.molstruc.2012.09.074

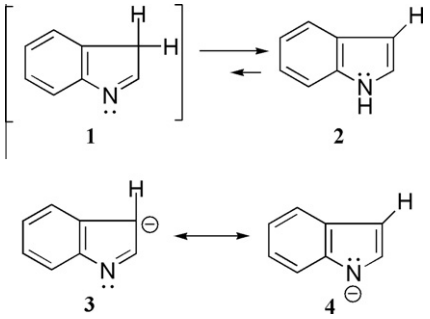

Scheme 1. Indolenine anion **3** achieves a longer life than indolenine **1**.

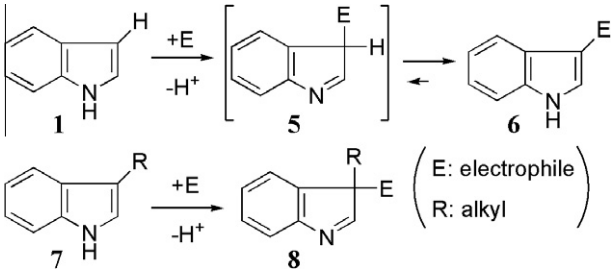

Scheme 2. A two-step procedure was suggested for the synthesis of 3,3-disubstituted indolenines.

β-allylation was not obtained under basic conditions. In fact, the typical β-alkylation of indole, which requires a basic environment, is less compatible with indolenine formation with many functionalized complex molecules.

Various palladium-catalyzed β-allylations have been examined for their ability to transform 3-substituted indoles into corresponding indolenines [8]. However, only one method has shown a broad range of applications that produced the desired indolenines from natural indole alkaloids with unprotected functional groups [9]. Rawal reported that yohimbine (**9**) reacted with the π-allyl Pd complex, which was generated *in situ* by the treatment of allyl methyl carbonate with Pd(0)-P(2-furyl)$_3$, to provide allylindolenine **10** in a 79% yield (Scheme 3). Reserpine (**11**) has been allylated to indolenine **12** in an approximately 1:1 ratio of diastereoisomers using the same procedure. The structure of **10** was tentatively assigned to (7*R*)-allyl yohimbine, based on its NMR spectral properties.

However, when we treated yohimbine (**9**) with methyl magnesium iodide and allyl bromide, C3-allyl yohimbine **10** (14%, dr 11:1) and N4-allyl yohimbine ammonium salt (44%) were obtained with recovered starting materials (16%). The allylation reaction of **9** under Rawal's conditions—2.5 mol% of Pd(0) treated with 15 mol% of P(2-furyl)$_3$, and with a longer reaction time (65 h)—yielded the isolation of two kinds of products (Scheme 4). An analysis of ^{1}H NMR data for them revealed that one of the two compounds was indolenine **10** and the other was an unknown compound **13** with an allyl moiety in a yohimbine structure. In the allylation of **11**, indolenine **12** was obtained in a 1:1 ratio. These results stimulated our interest in further study to characterize the unknown product **13**. Here, we describe the crystal structure of the indolenine **13** that resulted from the β-allylation of alkaloids, and discuss the origin of the stereoselectivity of the reaction.

2. Experiments and results

When the allylation reaction of **9** (0.226 g) was conducted, we achieved the successful resolution of a component that had only the unknown allyl yohimbine **13** (*ca.* 6.0 mg) by SiO_2 column chromatography. A colorless solid sheet appeared, indicating that **13** was very stable and pure, so that a crystal of **13** should be suitable for X-ray diffraction.

When this solid was dissolved in a hot mixture of CH_2Cl_2—CH_3CN (1:1), a crystal formed from the solution upon standing for *ca.* 3 days until the solvent was naturally evaporated. The structure of the crystal was examined by X-ray crystallography and determined to be (7*R*)-allyl yohimbine (Fig. 1, Table 1), which is 3*H*-indole (indolenine) with an axial allyl substitution at the C3 position.

In addition, we confirmed that ^{1}H and ^{13}C NMR of the crystal were different from those of the major compound, **10**, in the allylation. ^{1}H NMR spectra (Table 2 and Fig. 2) showed that the signals

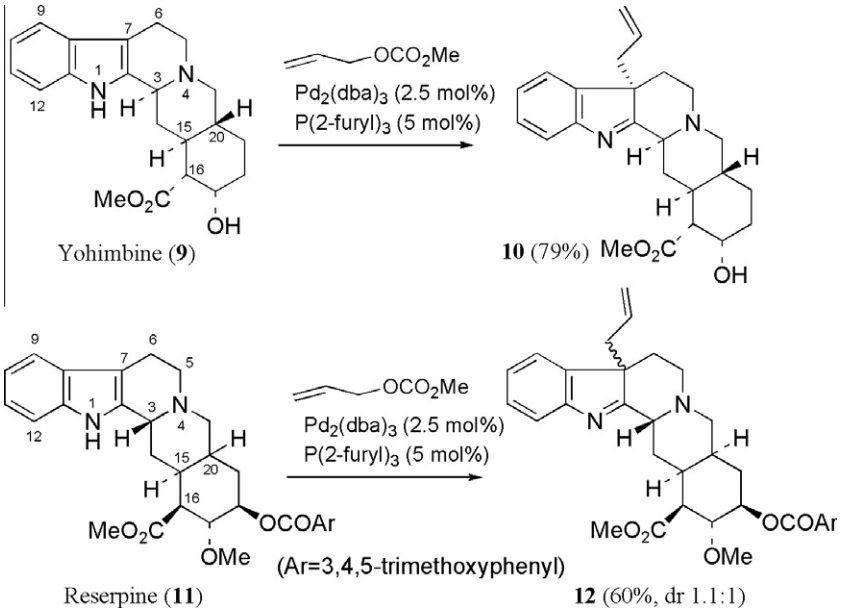

Scheme 3. (7*R*)-allyl yohimbine and (7*RS*)-allyl reserpine reported by Rawal's group.

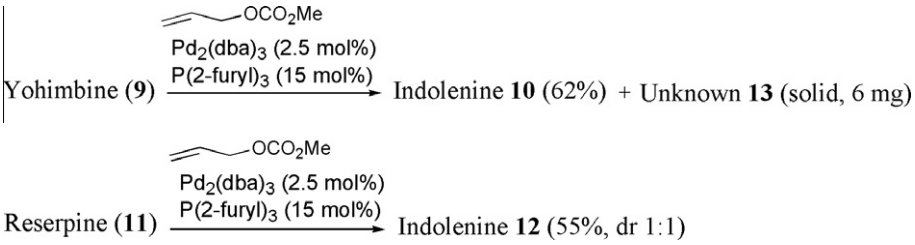

Scheme 4. The unknown compound **13** isolated in the *β*-allylation of yohimbine **9** in our research.

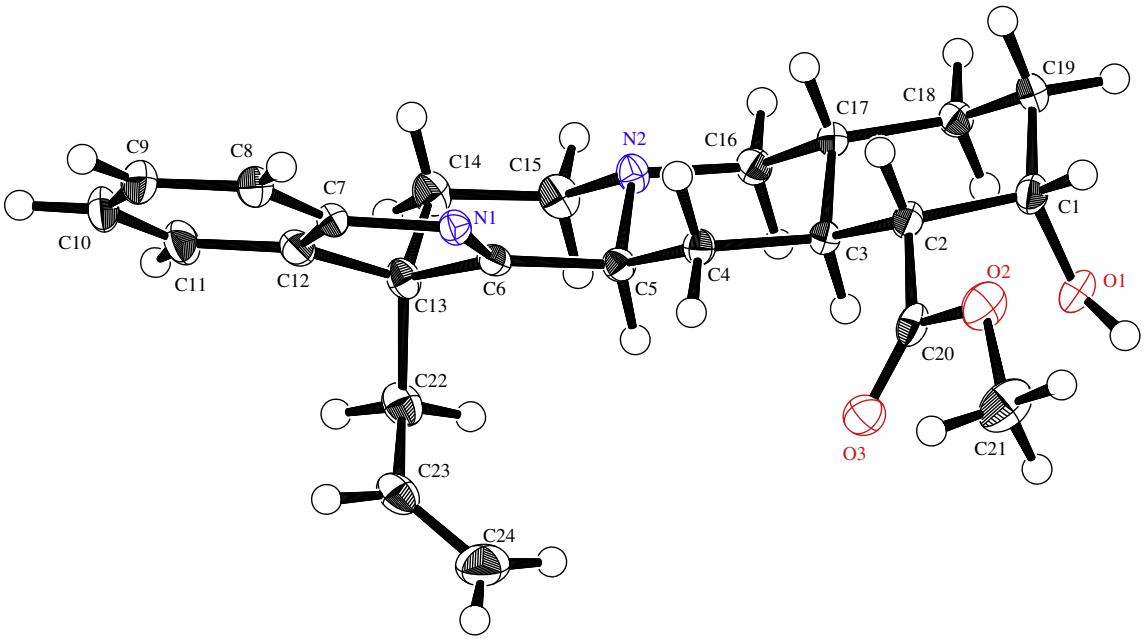

Fig. 1. ORTEP Diagram of **13**, assigned as an (7*R*)-allyl yohimbine structure. Selected crystal information is described in Table 1.

of four aromatic protons for **13** in the low-field region (>7.0 ppm) were upfield-shifted (0.13–0.04 ppm) for **10**. 1D NMR (^{1}H, ^{13}C and DEPT) spectra were complex and the assignment of the signals was achieved with the aid of the 2D NMR (^{1}H—^{1}H COSY, HMQC, HMBC, and NOESY) spectra shown in Table 3 and Fig. 3. NOESY cross-peaks were observed between the aromatic proton 3 and the olefinic proton 5 for both **10** and **13** (Fig. 2). Indolenines **10** and **13** were soluble in $CHCl_3$, but indolenine **10** was unstable and gradually decomposed both in air and in solution. Based on a survey of the ^{1}H NMR for **10** in $CDCl_3$, new signals other than those of **10** began to appear in the NMR tube 3 days after the **10** was freshly prepared.

These results confirm that the correct stereochemistry of **10** should have been (7*S*)-allyl yohimbine (Fig. 4). This was a unique example of disclosure of the X-ray crystal structure and stereochemistry of a free indolenine derivative, and could be employed in searching for the origin of stereoselectivity [10].

The oil state of **10** resisted the formation of a solid state, and, moreover, it was easily decomposed under various experimental conditions. In order to examine the process of stereoselective allylation, we attempted to explore the stable conformations of **9** and **11** by X-ray diffraction. Although the most favorable conformation of organic compounds in a solution was unclear, the crystal structures could suggest a plausible site, where allylating reagents would be accepted in a less-hindered place.

A crystal composed of two molecules of **9**, configured as if they were holding one another, was found. The lower molecule, visualized in Fig. 5, oriented both H(C5) and a lone pair of electrons (N2) to the axial position, as if adjacent rings seemed to connect in a *trans* manner, while the corresponding H(C26) in the upper molecule took the equatorial position, which resulted in *cis*-fusion of the rings.

A crystal of **11** was obtained from a CH_2Cl_2—CH_3CN solution and utilized for X-ray diffraction. The crystal structure of **11**, visualized in Fig. 4, had a conformation whereby a lone pair of electrons on N2 and all functional substitutes on C8, C9 and C10 were oriented to the equatorial position [11]. It was interesting that the bond length of 1.429 Å between C3 and C4 (Fig. 7, in blue[1]) in the indole (C12—C13 in Table 4, C16—C17 in Table 5) was the longest of any aromatic bonds of the indole units. This position of the bond seemed to release the stress of the five-membered ring of the indole units that had a plain structure due to π-conjugation. Such stress would disappear when the indole turned into an indolenine, whereby sp^3-hybridized carbon, C7, were connected with neighboring carbons C2 and C8 at *ca.* 1.5 Å (Fig. 7). The bond length of 1.293 Å between N1—C2 (Fig. 7 in red) in **13** was the shortest bond of the indolenine unit. In addition, this bond was shorter than the C=C olefinic bond (1.316 Å, C23—C24 in Fig. 1) in the allyl unit, and longer than the C=O double bond (1.203 Å, O3—C20 in Fig. 1). The bonding of N1—C2 was different in **9** and **13** when indole was converted to

[1] For interpretation of color in Figs. 6–8 and 10, the reader is referred to the web version of this article.

Table 1
Selected bond lengths, bond angles, and torsion angles of **13.**

Atoms	bond lengths (Å)	Atoms	bond angles (°)	Atoms	torsion angles (°)
N1—C6	1.2926(13)	N1—C6—C13	115.07(9)	N1—C6—C13—C12	0.39(11)
N1—C7	1.4336(14)	C6—C13—C12	99.70(8)	C4—C5—C6—N1	10.19(14)
N2—C5	1.4889(13)	C6—N1—C7	106.20(8)	C14—C13—C22—C23	168.93(8)
N2—C16	1.4688(14)	C8—C7—C12	122.07(10)	C3—C2—C20—C3	4.21(15)
N2—C15	1.4720(14)	C7—C12—C11	120.05(10)	C15—N2—C5—C6	−60.05(10)
C6—C13	1.5187(15)	C6—C13—C14	106.55(8)	O1—C1—C2—C3	−65.32(11)
C7—C8	1.3866(16)	C5—C6—C13	119.29(8)	C4—C3—C17—C16	−58.82(10)
C7—C12	1.3948(15)	C5—C2—C15	110.93(8)	C5—N2—C15—C14	63.29(11)
C8—C9	1.3953(16)	N2—C5—C6	104.81(8)	C1—C2—C20—C2	58.25(10)
C9—C10	1.3856(17)	N2—C15—C14	112.22(9)	N2—C5—C6—N1	112.32(11)
C10—C11	1.3950(18)	C5—N2—C16	110.07(8)	C5—C6—C13—C12	−171.49(9)
C11—C12	1.3883(15)	C7—C12—C13	107.34(9)	N1—C7—C12—C11	−178.27(9)
C12—C13	1.5037(15)	C6—C13—C22	112.32(11)	C13—C14—C15—C2	−55.74(12)
O3—C20	1.2030(13)	C13—C14—C15	111.43(8)	N2—C16—C17—C18	−173.63(8)

Table 2
^{1}H NMR Data for **10** and **13**.

^{1}H NMR 600 MHz[a]			
H[b]	**10**[c]	H[b]	**13**[c]
1	7.49 (d, *J* = 8.4, 1H)	1	7.62 (d, *J* = 7.2, 1H)
2	7.26 (dd, *J* = 7.8, 1.8, 1H)	2	7.30 (dd, *J* = 7.2, 0.6, 1H)
3	7.22 (d, *J* = 6.6, 1H)	3	7.27 (d, *J* = 7.2, 1H)
4	7.14 (td, *J* = 7.8, 1.2, 1H)	4	7.18 (t, *J* = 7.2, 1H)
5	5.19 (ddt, *J* = 17, 10, 6.6, 1H)	5	5.11 (ddt, *J* = 16, 9.6, 6.6, 1H)
6	4.89 (dd, *J* = 17, 1.8, 1H)	6	4.91 (d, *J* = 17, 1H)
7	4.83 (dt, *J* = 9.6, 1.2, 1H)	7	4.84 (dd, *J* = 9.6, 1.2, 1H)
8	4.15 (d, *J* = 1.8, 1H)	8	4.17 (s, 1H)
9–11[d]	3.70 (s, 3H)	9–11 [d]	3.74 (s, 3H)
12	3.50 (br s, 1H)	12	3.07 (dd, *J* = 11, 2.4, 1H)
13	3.26 (dd, *J* = 11, 2.4, 1H)	13	2.94 (br s, 1H)
14	3.02 (dd, *J* = 14, 7.2, 1H)	14	2.90 (dd, *J* = 11, 3.6, 1H)
15	2.95 (ddd, *J* = 12, 9.0, 3.6, 1H)	15	2.74 (ddd, *J* = 12, 4.2, 1.8, 1H)
16/17[e]	2.86–2.82 (m, 2H)	16	2.69 (dt, *J* = 12, 2.4, 1H)
18	2.42 (dt, *J* = 13, 8.4, 1H)	17[h]	2.61 (dd, *J* = 14, 6.6, 1H)
19	2.27 (dd, *J* = 11, 1.8, 1H)	18[h]	2.58 (dd, *J* = 14, 7.8, 1H)
20	2.22 (dt, *J* = 11, 7.8, 1H)	19	2.36 (dd, *J* = 11, 1.8, 1H)
21	2.03 (t, *J* = 11, 1H)	20	2.24 (dt, *J* = 14, 2.4, 1H)
22/23[f]	1.98–1.94 (m, 2H)	21	2.19 (t, *J* = 11, 1H)
24	1.91 (dt, *J* = 13, 3.0, 1H)	22	2.05 (dt, *J* = 13, 3.0, 1H)
25	1.60–1.53 (m, 1H)	23/24[i]	1.99–1.90 (m, 2H)
26	1.56–1.50 (m, 1H)	25	1.75 (q, *J* = 12, 1H)
27/28[g]	1.53–1.47 (m, 2H)	26	1.59–1.49 (m, 1H)
29	1.48–1.44 (m, 1H)	27	1.56–1.45 (m, 1H)
30	1.35 (dq, *J* = 12, 3.0, 1H)	28	1.46 (td, *J* = 13, 4.8, 1H)
		29	1.42 (qd, *J* = 12, 3.6, 1H)
		30	1.36–1.34 (m, 1H)

[a] In $CDCl_3$. Internal reference: $CHCl_3$ (7.24 ppm).
[b] Assignment of protons in Fig. 2.
[c] In δ(ppm). Multiplicity, *J* (Hz) and a number of protons in parentheses.
[d] The protons 9–11 for **10** and **13** are equivalent and appear as a singlet at 3.70 and 3.74 ppm, respectively.
[e] The protons 16 and 17 for **10** overlap and appear as a multiplet at 2.86–2.82 ppm.
[f] The protons 22 and 23 for **10** overlap and appear as a multiplet at 1.98–1.94 ppm.
[g] The protons 27 and 28 for **10** overlap and appear as a multiplet at 1.53–1.47 ppm.
[h] The protons 17 and 18 for **13** have been tentatively assigned the doublet of doublets at 2.62 ppm to 17 and that at 2.57 ppm to 18.
[i] The protons 23 and 24 for **13** overlap and appear as a multiplet at 1.99–1.90 ppm.

indolenine (Fig. 7). These results suggest that the indolenines underwent conjugated double bonding (Ph—N=C) in N1—C2, though indoles underwent resonance bonding in the corresponding N1—C2 as part of an aromatic ring.

3. Discussion

Despite experimental efforts to form a solid, **10** and **12** remained in an oil state. The majority of their conformations, therefore, were examined by computational optimization. A calculation was performed at the Hartree–Fock/3-21G(∗) level utilizing the Spartan program. (Spartan' 02 for Windows, Wavefunction, Inc.).

The computational model of **10**, as shown in Fig. 8, had a boat conformation (blue-highlighted) that contained the torsional strain of the eclipsing CH_2—CH_2 group in the C2—C3—N4—C5—C6 heterocycle. The corresponding part of **13** was composed of chair conformation rings, as shown in Fig. 9, where the allyl substitution resulted in 1,3-diaxial interactions. This computational conformation for **13** had good agreement with the crystal found in Fig. 1. The conformation for **10** had good agreement with the NOESY experiments. The allylic proton 5 was close to the aromatic proton

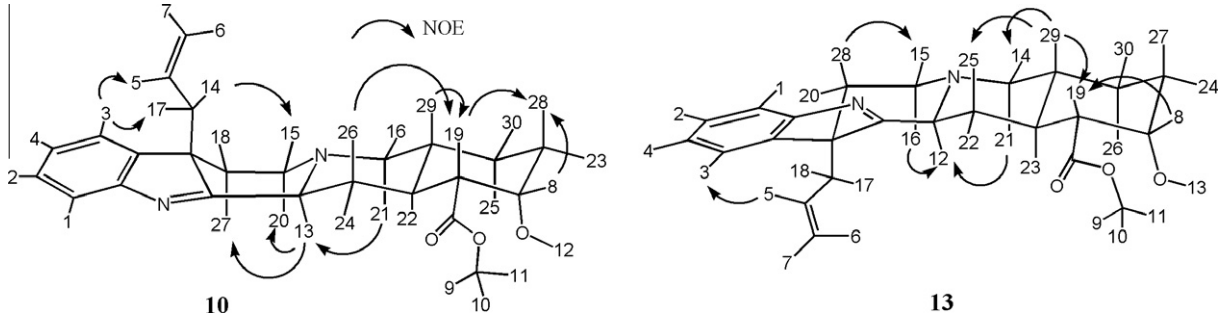

Fig. 2. ^{1}H NMR assignment for **10** and **13**, and observation of selected NOEs.

Table 3
^{13}C NMR Data for **10** and **13**.

^{13}C NMR 150 MHz[a]					
10			**13**		
C[b]	^{1}H—^{13}C coupling[c]	δ (ppm)	C[b]	^{1}H—^{13}C coupling[c]	δ (ppm)
1	C	188.4	1	C	185.0
2	C	175.9	2	C	175.6
3	C	154.9	3	C	154.7
4	C	144.4	4	C	144.0
5	CH	133.1	5	CH	131.4
6	CH	127.6	6	CH	127.8
7	CH	125.1	7	CH	125.2
8	CH	122.0	8	CH	121.9
9	CH	120.1	9	CH	120.9
10	CH_2	118.1	10	CH_2	118.5
11	CH	66.5	11	CH	66.9
12	CH	65.9	12	CH_2	61.8
13	CH_2	60.3	13	CH	60.8
14	C	56.7	14	C	56.4
15/16[d]	CH or CH_3	52.1	15/16 [d]	CH or CH_3	52.2
16/15 [d]	CH or CH_3	51.9	16/15 [d]	CH or CH_3	51.9
17	CH_2	49.4	17	CH_2	50.6
18	CH_2	41.8	18	CH	40.3
19	CH	40.4	19	CH_2	37.3
20	CH	37.2	20	CH	36.2
21	CH_2	33.8	21	CH_2	34.5
22/23 [e]	CH_2	31.1	22	CH_2	31.6
23/22 [e]	CH_2	29.8	23	CH_2	31.3
24	CH_2	23.2	24	CH_2	23.1

[a] In $CDCl_3$ internal reference: $CHCl_3$ (77.0 ppm).
[b] Assignment of carbons in Fig. 3.
[c] Determined by DEPT 135.
[d] Chemical shifts of carbons 15 and 16 are too close to assign.
[e] Chemical shifts of carbons 22 and 23 are too close to assign.

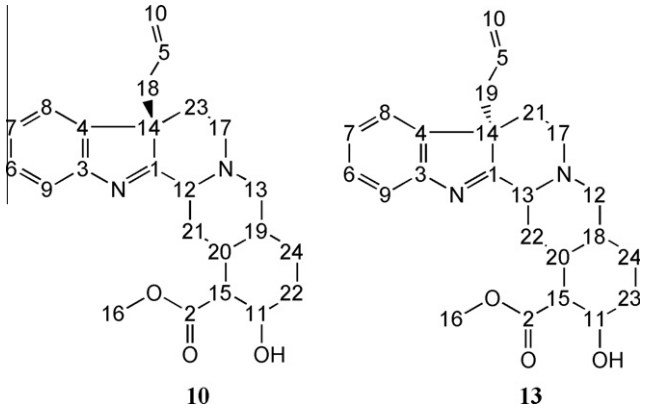

Fig. 3. ^{13}C NMR assignment for **10** and **13**. Chemical shifts of the signals for 15 and 16 are too close to assign, as with those for 22 and 23.

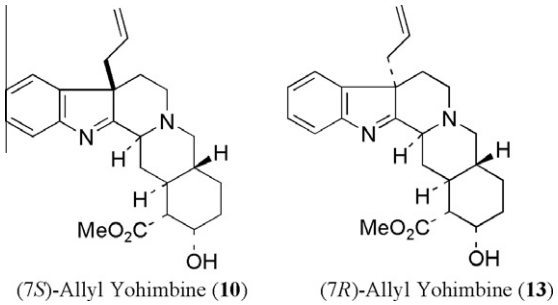

Fig. 4. The correct structures for **10** and **13** are proposed based on X-ray analysis.

3 (H—C9), in both **10** (Fig. 8) and **13** (Fig. 9). Form **13** was 10.5 kJ/mol lower in energy than form **10**. In addition, the reverse reaction, turning indolenine into indole, has not been observed under such allylation conditions. Under these circumstances, the terms "thermodynamic control" or "product development control" do not describe the stereoselectivity [12]. An alternative description, "kinetic control" or "steric approach control," which predicts the transition state geometry from the starting indole, is suggested for this allylation.

The crystal structure of **9** in Fig. 3 was in good agreement with the computationally optimized model in Fig. 10 (see Section 5.2 in Section 5).

Under allylation at the C7 position of **9**, the favored side of the approach for the π-allyl Pd complex should be the less-hindered side of the molecule. Two pseudoaxial hydrogens, shown in red, orient toward the down side in Fig. 10, occupying the C3 and C5 positions in the structure, which are in a 1,3 relationship against C7. They can generate steric interactions as 1,3-diaxial interactions in a half-chair cyclohexene ring when the π-allyl Pd complex coordinates on the bottom face of the indole molecule. Approaching from the top of the indole molecule, on the other hand, requires C6 pseudoaxial hydrogen (in blue) to rotate into a position that gives almost a half-boat arrangement of the cyclohexene ring. Steric repulsion that is similar to a 1,4-transannular interaction may be lower between N4 (a lone pair of electrons) and the approaching allyl moiety. The result of this allylation reaction for **9** indicates that a C6 carbon has sufficient flex to rotate and interconvert into a conformer, as illustrated in Fig. 8. Given the fact that the stereoselective ratio of products does not seem to match the thermodynamic prediction, it must be influenced by kinetic factors. The stereochemistry of the products is determined mainly by a steric effect in the transition state, which resembles the reactants in geometry when the π-allyl Pd unit comes close to the reactive position. Consequently, **10** was produced as a major stereoisomer through coordination of the π-allyl Pd complex with the less-hindered *pro-S* side. A proposed mechanism of the Pd-mediated

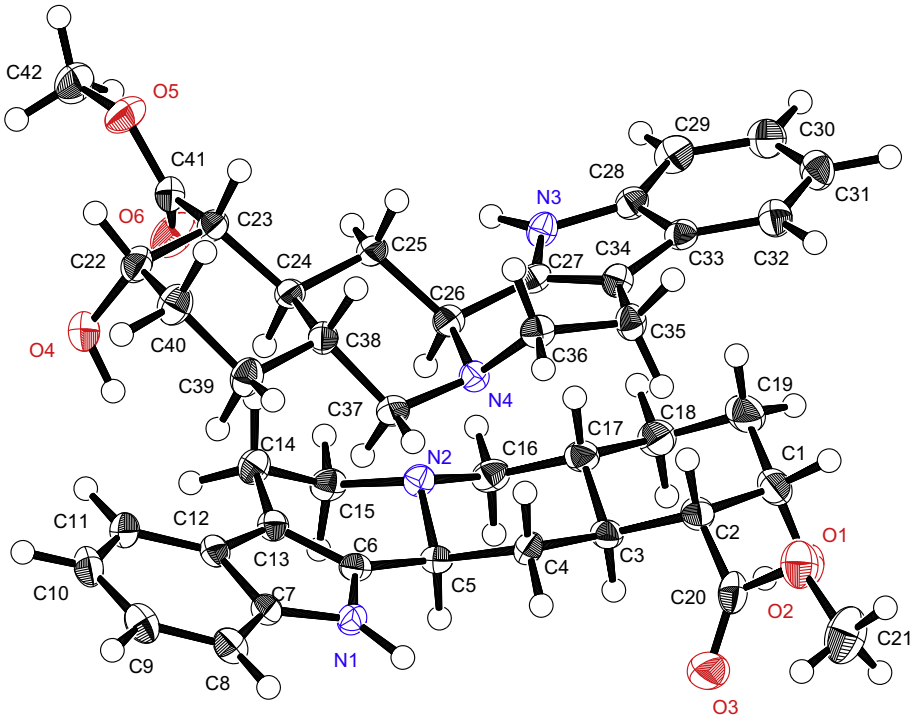

Fig. 5. ORTEP Diagram of **9**. Selected crystal information is described in Table 4.

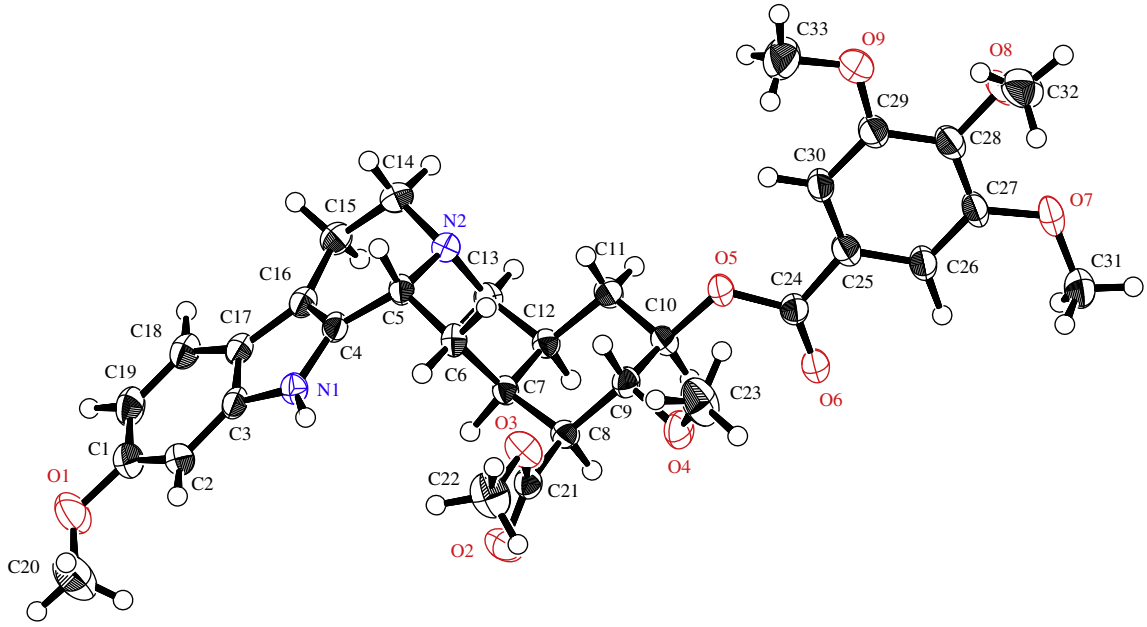

Fig. 6. ORTEP Diagram of **11**. Selected crystal information is described in Table 5.

allylation of **9** is presented in Scheme 5 [13]. Allyl methyl carbonate and activated Pd(0) species formed the π-allyl Pd complex **14**, which underwent nucleophilic attack by the indolenium anion **15**. During the process of the formation of **14**, the methoxide ion **16** was generated by decomposition of the carbonate ion **17**, and it reacted with **9** as a proton base. The anion **15** approached the positively charged **14** from the less-hindered *pro-S* side, resulting in the (7*S*)-selective allylation of product **10**.

Product **9** had a structure with fused rings at the *cisoid*-3, 15 (5,3)-ring junctions [14]. In the allylation of **9**, sluggish reaction rates were observed when the reaction was conducted at −40 to 0 °C, and decomposition of the products resulted in low yields at temperatures above 30 °C. Even at room temperature, 69 mg of a 2:1 mixture of **10** and **13** was lost and turned into 32 mg of a 7.7:1 mixture of both indolenines after a 24-h exposure to the general allylation conditions. This means that **10** was less stable than **13** in the reaction process, so that the longer reaction times caused higher ratios for the diastereomers, due to the selective decomposition of **10**. The reaction time, more than 65 h under our initial conditions, seemed sufficient for isolation of the crystal

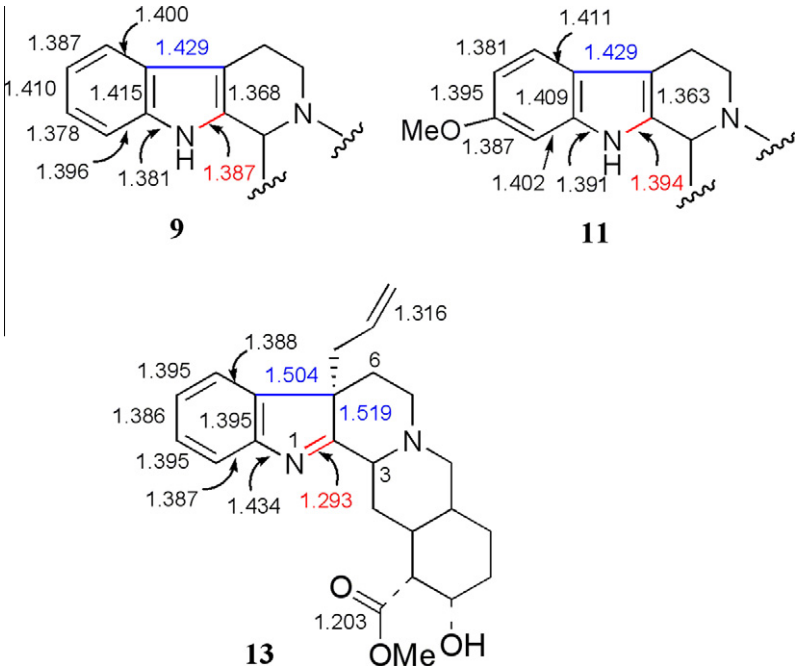

Fig. 7. Selected bond lengths for **9**, **11**, and **13**.

Table 4
Selected bond lengths, bond angles, and torsion angles of **9**.

Atoms	bond lengths (Å)	Atoms	bond angles (°)	Atoms	torsion angles (°)
N1—C6	1.387(2)	N1—C6—C13	109.30(14)	O1—C1—C2—C20	50.42(19)
C6—C13	1.368(2)	C6—C13—C12	107.61(15)	C15—N2—C5—C6	−49.96(16)
C12—C13	1.429(2)	N3—C27—C34	109.34(15)	C4—C3—C17—C16	−54.67(17)
N1—C7	1.381(2)	C27—C34—C33	107.66(15)	C36—N4—C26—C27	43.60(17)
N2—C5	1.481(2)	C6—N1—C7	108.66(14)	C26—N4—C36—C35	−68.75(17)
N3—C27	1.395(2)	C5—N2—C16	109.20(13)	C37—N4—C26—C25	46.11(17)
C27—C34	1.362(2)	C27—N3—C28	108.41(14)	C4—C5—C6—N1	−43.20(2)
N3—C28	1.379(2)	N1—C7—C12	107.80(14)	N1—C6—C13—C12	0.59(18)
N4—C26	1.488(2)	N3—C28—C29	130.50(17)	N1—C7—C12—C13	−0.45(17)
O6—C	1.196(2)	N1—C6—C5	125.28(15)	C5—C6—C13—C14	0.9(2)

Table 5
Selected bond lengths, bond angles, and torsion angles of **11**.

Atoms	bond lengths (Å)	Atoms	bond angles (°)	Atoms	torsion angles (°)
N1—C4	1.394(2)	C6—C7—C8	113.40(15)	C5—C4—C16—C15	5.80(3)
N1—C3	1.391(3)	C10—O5—C24	117.25(15)	C14—N2—C13—C12	173.29(16)
C4—C16	1.363(2)	C4—C16—C17	107.52(14)	C8—C7—C12—C13	−178.08(15)
C16—C17	1.429(3)	C5—N2—C13	111.83(13)	C13—N2—C14—C15	61.20(2)
O2—C21	1.202(2)	N1—C4—C16	109.34(18)	C5—N2—C14—C15	−63.50(2)
O6—C24	1.200(2)	N2—C5—C4	109.50(15)	C4—C5—C6—C7	74.55(19)

13. This experimental result supported the hypothesis that stereoselective indole β-allylation via the π-allyl Pd complex could be controlled by a steric effect that originated in the initial conformation of the molecule. However, contemporaneous improvement of both selectivity and yield proved difficult, because the reaction proceeded slowly, which promoted the instability of products in cooperation with the active π-allyl Pd complex, even in the reaction medium.

In order to adopt the stereochemical feature that dominates the allylation reaction of **11**, computational optimization among conformers was carried out (Fig. 11). The conformer **18**, which resembles the observation in X-ray diffraction (Fig. 6), appeared to be more favorable than conformer **19**, by 3.31 kJ/mol. Allylation for **11** took place from both sides of conformer **18** competitively, producing two stereoisomers in a ratio of *ca.* 1:1. When the π-allyl Pd complex was coordinated on the top of **18** around C7 (C16), two axial hydrogens (in red) on C3 (C14) and C5 (C5) occupied the space for allyl introduction by 1,3-diaxial interactions [15]. On the bottom, two axial hydrogens (in blue) on C15 (C7) and C21 (C13), which were oriented toward a concavity in the structure,

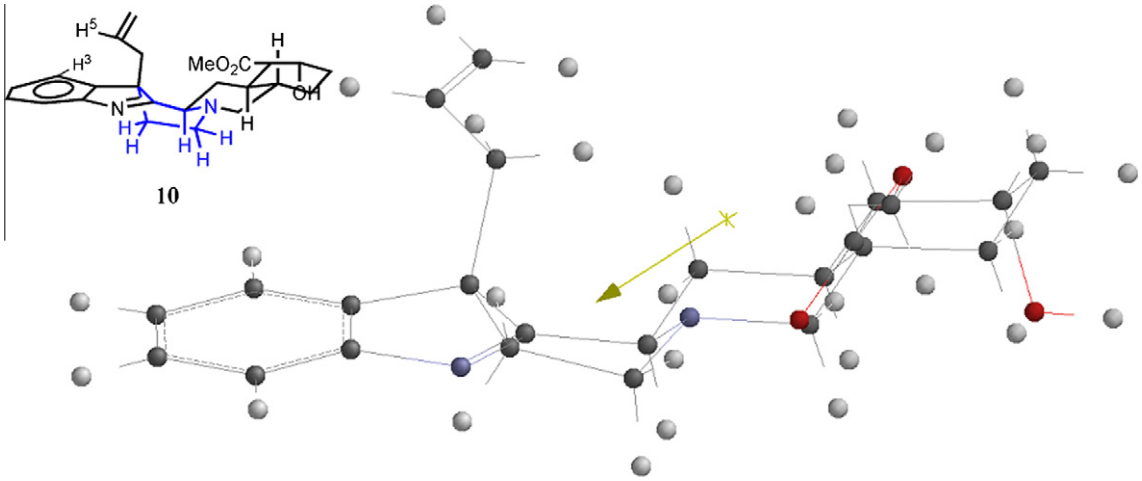

Fig. 8. A computational method was used to propose an optimized conformation for (7*S*)-allyl yohimbine **10**.

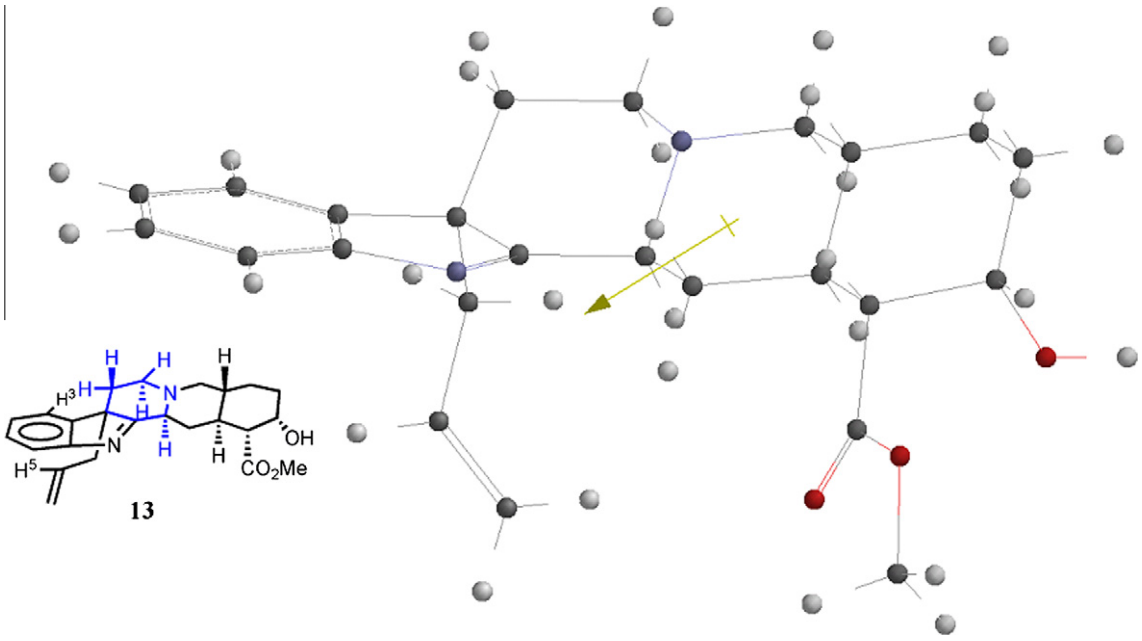

Fig. 9. A computational method was used to propose an optimized conformation for (7*R*)-allyl yohimbine **13**.

can disturb the approach by transannular strains. The latter steric effect occurs only in reserpine-like fused systems, due to *transoid*-3, 15 (5,7)-ring junctions.

Stable conformations for allylated reserpines were calculated to rationalize the outcome in the reaction. Based on the conformations of **18** and **19**, four representatives were selected and utilized to identify the destabilization arising from steric strain. Conformations of **20** and **21** were proposed as optimized geometries for (7*S*)-allyl reserpine (Fig. 12). This suggested that conformer **20** was more stable than conformer **21** when the allyl unit on C(7) was allowed to orient with the least 1,3-allylic strain. An extremely large gap existed between conformers **22** and **23** for (7*R*)-allyl reserpine, and the chair conformation **23** was stable because **23** can avoid the torsional strain of the eclipsing CH_2—CH_2 group and the 1,4-transannular interaction contained in the crowded-boat conformation **22** (Fig. 13).

The energy ranking of conformations **20**–**23** was on the order of **22** > **23** > **21** > **20** (**20** is the lowest). Therefore, the most favorable conformations for (7*S*)- and (7*R*)-allyl reserpine were found to be in the states of conformers **20** and **23**, respectively. Although the energy gap between **20** and **23** was large enough to predict exclusive production of (7*S*)-allyl reserpine, the ratio of diastereomers was steady at 1:1 even when yields went up and down under various reaction times. This implied that the allylation reaction for **11** was controlled by the steric effect of the molecular structure of **11**.

4. Conclusion

The structure of **13** was characterized by X-ray crystallography as an (7*R*)-allyl indolenine derived from the natural indole alkaloid **9**. Favorable conformations for **13**, **9** and **11** were proposed by X-ray diffraction, and supported by computational calculation. These results help to explain why the stereoselective approach of the π-allyl Pd complex to **9** by a steric effect dominated the outcome of the *β*-allylation reaction. When applied to **11**, both sides of con-

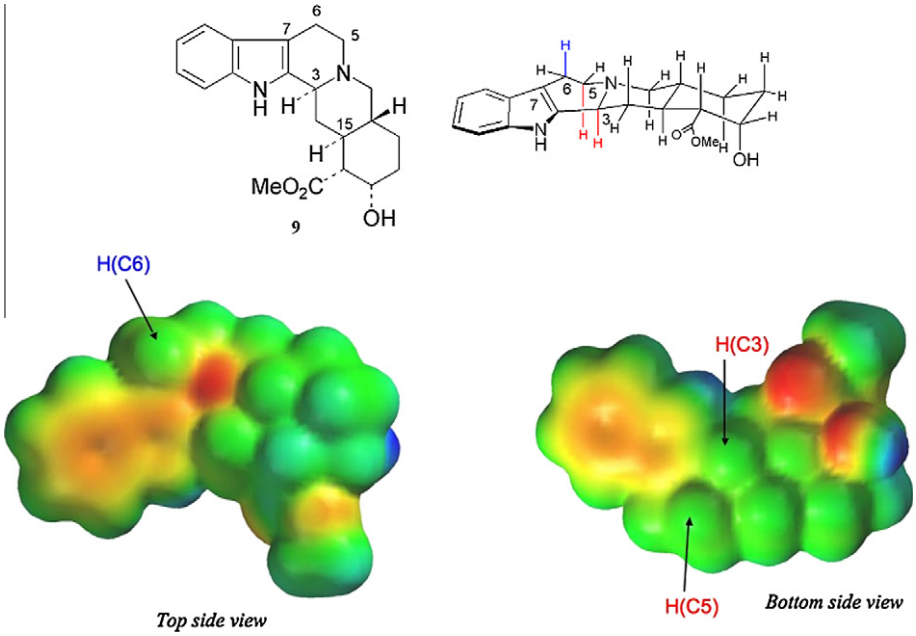

Fig. 10. A computational method was used to propose an optimized conformation for **9**.

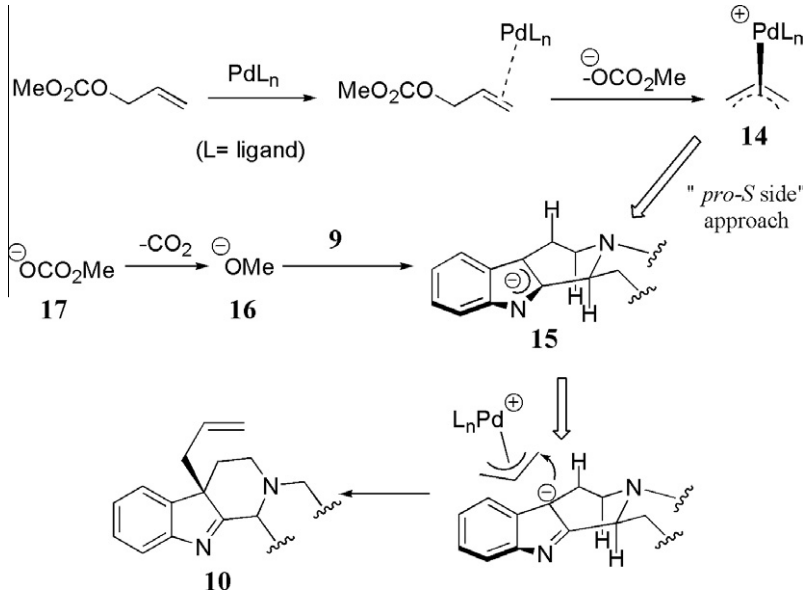

Scheme 5. A proposed mechanism for the Pd-mediated allylation of **9**.

former **18** had no determinative steric factors by which the C(7) position was blocked from the attack of the allyl unit. Conformer **23** of (7*R*)-allyl reserpine resulted from the flipping of conformer **22**, which was initially derived from the attack of the π-allyl Pd complex at the *pro-R* side of **11**.

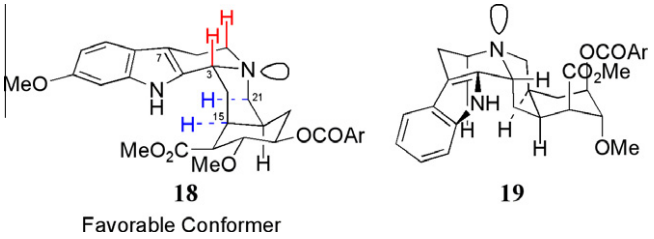

Fig. 11. Conformation of **18** is present as a structure of **11** with lower energy.

5. Experimental details

5.1. Materials and techniques

Yohimbine hydrochloride was purchased from Aldrich Chemical Co., Inc. Reserpine was purchased from Tokyo Chemical Industry Co., Ltd. Tris(dibenzylideneacetone)dipalladium(0) was purchased from Strem Chemicals, Inc. Tris(2-furyl)phosphine was purchased from Wako Pure Chemical Industries, Ltd. Allyl methyl carbonate was freshly synthesized (vide infra). Anhydrous CH_2Cl_2 was purchased from Kanto Chemical Co., Inc. Column chromatography was carried out using Cica 60 (spherical/63–210 μm) silica gel. Reactions and chromatography fractions were analyzed employing precoated silica gel 60 F_{254} plates (Merck).

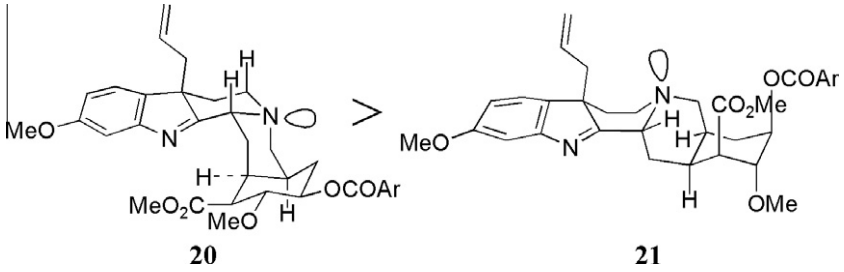

20 21

Fig. 12. Conformation of **20** is present as a structure of (7*S*)-allyl reserpine with lower energy.

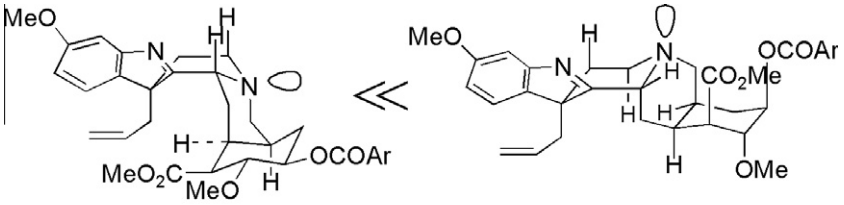

22 23

Fig. 13. Conformation of **22** is present as a structure of (7*R*)-allyl reserpine with lower energy.

5.1.1. Synthesis of allyl methyl carbonate

To a mixture of pyridine (24 mL, 0.30 mol) and allyl alcohol (15 mL, 0.22 mol) was added methyl chloroformate (17 mL, 0.22 mL) at 0 °C very slowly. The resultant mixture was stirred for 12 h, and then poured onto water in a beaker. Biphasic solutions were separated by decantation. The separated organic layer was washed with saturated $CuSO_4$ (aq. 30 mL × 2), water (20 mL) and saturated NaCl (aq. 20 mL). The resultant liquid was dried over Na_2SO_4 to give allyl methyl carbonate (11 g, 0.095 mol) as a colorless liquid, which was used for the Pd-catalyzed allylation reaction without further purification. ^{1}H NMR (400 MHz): δ 5.94 (ddt, *J* = 11, 10, 5.6 Hz, 1H), 5.36 (dq, *J* = 17, 1.2 Hz, 1H), 5.27 (dq, *J* = 12, 1.6 Hz, 1H), 4.64 (dt, *J* = 5.6, 1.2 Hz, 2H), 3.80 (s, 3H); ^{13}C NMR (100 MHz) δ 155.4, 131.5, 118.5, 68.2, 54.5.

5.1.2. Synthesis of (7R)-ally yohimbine (13)

To a 300 mL Erlenmeyer flask, yohimbine hydrochloride (13.7 g) was allowed to settle, and saturated $NaHCO_3$ (aq., 150 mL) was added in many portions. The solution was vigorously stirred in an ice-cooled bath for 5 h, and passed through a filter paper under suction. The white cake on the filter was washed with distilled water, dried with paper, pulverized and then dried in vacuo at 50 °C for 4 days to give a white powder (13.0 g), which was used for the next allylation step.

A solution of $Pd_2(dba)_3$ (14.6 mg, 16.0 μmol) and P(2-furyl)$_3$ (22.2 mg, 95.7 μmol) in CH_2Cl_2 (6.6 mL) was degassed and stirred for 30 min. Allyl methyl carbonate (0.145 mL, 1.28 mmol) was added, and the resultant green solution was stirred for an additional 30 min. Dried yohimbine powder (226 mg, 0.638 mmol) was finally added in one portion under a nitrogen flow. The solution was stirred for 65 h until the green suspension was turned to a clear greenish solution. The solvent was removed to give a crude oil. Purification by flash silica gel column chromatography (CH_2Cl_2/MeOH = 98/2–97/3) provided two separated components in white solid (**13**, 6 mg) and yellow oil (**10**, 155 mg).

Data for **13**[2]: mp 189–192 °C; R_f 0.25 (98:2 CH_2Cl_2:MeOH), R_f 0.31 (3:1 CH_3Cl:CH_3CN); $[\alpha]_D^{27}$+174 (0.287, $CHCl_3$); IR: 3343, 2940, 2784, 2740, 1743, 1613, 1586, 1435, 1287, 1202, 1143, 1006, 960, 923, 760 cm^{-1}; HRMS (FAB$^+$) Calcd for C24H31N2O3 (M + H$^+$): 395.2335, Found: 395.2331.

[2] ^{1}H and ^{13}C NMR data for **10** and **13** are reported in Tables 2 and 3, respectively.

5.2. Computational methods

Density functional theory (DFT) with the B3LYP functional and 6-31G(d) basis set was also used for the calculation of **9**, but the calculation time was longer than when using Hartree–Fock (HF)/3-21G(∗). Then, we compared the computational optimized structures {DFT or HF} and the crystal structure {ORTEP} for **9**. To assess the differences between a computational model and a crystal structure in the solid state, the selected bond lengths and bond angles for **9** are listed in Table 6. Both computational structures were in good agreement with the crystal structure. The largest difference in bond length was observed for the double bond of C2—C7 (cryst.: 1.346 Å, HF: 1.368 Å). We determined by this outcome that the HF level was sufficient, and it was then utilized for the calculation of **10**, **11**, **13**, **18**, **19**, **20**, **21**, **22**, and **23**.

Table 6
Selected bond lengths and bond angles for **9**.

Bond lengths (Å)	The X-ray cryst.[b]	The HF model[b]	The DFT model[b]
N1—C2	1.387	1.386	1.386
C3—N4	1.481	1.474	1.472
N1—C13	1.381	1.380	1.384
C2—C7	1.368	1.346	1.371
C7—C8	1.429	1.446	1.439
C6—C7	1.497	1.501	1.499
C2—C3	1.498	1.497	1.501
Bond angles (°)			
N1—C2—C7	109.30	109.97	109.73
C2—C7—C8	107.61	107.15	107.13
C2—N1—C13	108.66	108.68	109.02
N1—C13—C8	107.80	107.51	107.35
N1—C2—C3	125.28	124.24	124.73

[b] The X-ray crystal (ORTEP) and the HF model are presented in Figs. 5 and 10, respectively.

Acknowledgments

We thank Dr. Concepción López for useful discussions and Mr. Syohei Katao for assistance with the X-ray analysis. This work was supported by KAKENHI (20890129).

Appendix A. Supplementary material

Supplementary data (Characterization data and NMR spectra for 10 and 13, and crystallographic data for 13, 9 and 11.) associated with this article can be found, in the online version, at http://dx.doi.org/10.1016/j.molstruc.2012.09.074.

References

[1] J.L. Julian, E.W. Meyer, H.C. Printy, in: R.C. Elderfield (Ed.), Heterocyclic compounds, vol. 3, John Wiley & Sons, New York, 1952, pp. 74–114.
[2] (a) R.J. Sundberg, in: Indoles, Academic Press, London, 1996;
(b) J.E.E. Saxton, Indoles, vol. 25, John Wiley & Sons, New York, 1983 (Part 4);
(c) M. Hesse, in: Alkaloids, VCH, Weinheim, 2002, pp. 14–30.
[3] Recent Contributions on this area: (a) G.L. Adams, P.J. Carroll, A.B. Smith III, J. Am. Chem. Soc. 134 (2012) 4037–4040;
(b) L.-M. Li, T. Yang, Y. Liu, J. Liu, M.-H. Li, Y.-T. Wang, S.-X. Yang, Q. Zou, G.-Y. Li, Org. Lett. 14 (2012) 3450–3453;
(c) L. Liu, L. Zhang, Angew. Chem. Int. Ed. 51 (2012) 7301–7303;
(d) A. Berger, H. Fasshuber, J. Schinnerl, L. Brecker, H. Greger, Phytochem. Lett. 5 (2012) 558–562;
(e) J.D. White, Y. Li, D.C. Ihle, J. Org. Chem. 75 (2010) 3569–3577.
[4] (a) S. Zhu, D.W.C. MacMillan, J. Am. Chem. Soc. 134 (2012) 10815–10818;
(b) Z. Béni, V. Háda, Z. Dubrovay, C. Szántay Jr., J. Pharm. Biomed. Anal. 69 (2012) 106–124.
[5] (a) S.F. Völker, C. Lambert, Chem. Mater. 24 (2012) 2541–2553;
(b) C. López, C. Moya, P.K. Basu, A. González, X. Solans, M. Font-Bardía, T. Calvet, E. Lalinde, M.T. Moreno, J. Mol. Struc. 999 (2011) 49–59;
(c) S. Sajjadifar, H. Vahedi, A. Massoudi, O. Louie, Molecules 15 (2010) 2491–2498.
[6] (a) M. Gerowska, L. Hall, J. Richardson, M. Shelbourne, T. Brown, Tetahedron 68 (2012) 857–864;
(b) M.S.T. Gonçalves, Chem. Rev. 109 (2009) 190–212;
(c) A. Fegan, P.S. Shirude, S. Balasubramanian, Chem. Comm. (2008) 2004–2006;
(d) Y. Nagao, T. Sasaki, K. Kozawa, T. Urano, Dyes Pigm. 73 (2007) 344–352;
(e) X. Chen, X. Peng, A. Cui, B. Wang, L. Wang, R. Zhang, J. Photochem. Photobiol., A 181 (2006) 79–85;
(f) C.A. Bertolino, A.M. Ferrari, C. Barolo, G. Viscardi, G. Caputo, S. Coluccia, Chem. Phys. 330 (2006) 52–59;
(g) P. Chen, S. Sun, Y. Hu, Z. Qian, D. Zheng, Dyes Pigm. 41 (1999) 227–231;
(h) H.-H. Johannes, W. Grahn, I. Dix, P.G. Jones, Sect. C: Cryst. Struct. Commun. C53 (1997) 1432–1434;
(i) Q. Li, B.-X. Peng, Molecule 2 (1997) 91–98;
(j) G.T. Pilyugin, Z. Ya, Zh. Org. Khim. 25 (1955) 2237–2239.
[7] (a) S. Nunomoto, Y. Kawakami, Y. Yamashita, H. Takeuchi, S. Eguchi, J. Chem. Soc. Perkin Trans. 1 (1990) 111–114;
(b) M. Nakazaki, Bull. Chem. Soc. Jpn. 34 (1961) 334–337;
(c) T. Hoshino, Justus Liebigs Annalen der Chemie 500 (1933) 35–42.
[8] (a) M. Kimura, M. Futamata, R. Mukai, Y. Tamaru, J. Am. Chem. Soc. 127 (2005) 4592–4593;
(b) B.M. Trost, J. Quancard, J. Am. Chem. Soc. 128 (2006) 6314–6315.
[9] N. Kagawa, J.P. Malerich, V.H. Rawal, Org. Lett. 10 (2008) 2381–2384 (and references there in).
[10] It should be noted that "free indolenine" has less stability against air and light than indolenium salts.
[11] G. Stork, P.C. Tang, M. Casey, B. Goodman, M. Toyota, J. Am. Chem. Soc. 127 (2005) 16255–16262.
[12] (a) H.O. House, in: Modern Synthetic Reactions, second ed., W. A. Benjamin, Inc., Philippines, 1972, pp. 54–71 (Chapter 2);
(b) S.R. Buxton, S.M. Roberts, in: Guide to Organic Stereochemistry, Addison Wesley Longman, England, 1996, pp. 11–71.
[13] For Pd-mediated allylation mechanism: (a) M. Patil, W. Thiel, Chem. Eur. J. 18 (2012) 10408–10418;
(b) F. Manjolinho, M.F. Grünberg, N. Rodríguez, L.J. Gooβen, Eur. J. Org. Chem. (2012) 4680–4683;
. For reviews:(c) J.T. Mohr, B.M. Stoltz, Chem. Asian. J. 2 (2007) 1476–1491;
(d) C. Hyland, Tetrahedron 61 (2005) 3457–3471.
[14] The numbers corresponding to the ORTEP in figure ure5 are given in parentheses.
[15] The numbers corresponding to the ORTEP in figure ure6 are given in parentheses.